Optimizing Photovoltaic Efficiency of a Dye-Sensitized Solar Cell (DSSC) by a Combined (Modelling-Simulation and Experimental) Study

D. Kumar[1], K. P. S. Parmar[2], P. Kuchhal[2]*

[1]Department of Electrical and Electronics Engineering, University of Petroleum and Energy Studies (UPES), 248007 Dehradun, India
[2]Department of Applied Sciences, University of Petroleum and Energy Studies (UPES), 248007 Dehradun, India

E-mail: d.kumar@ddn.upes.ac.in

kpsparmar@ddn.upes.ac.in

*Corresponding author. E-mail: pkuchhal@ddn.upes.ac.in

Received: 17.12.2019 Accepted:06.02.2020

Abstract: A comparative investigation involving experimental and modelling-simulation is carried out to maximize the photovoltaic conversion efficiency (η) of a DSSC device assembled using N719 dye, an iodide redox liquid electrolyte and TiO_2 electrode. The measured current density-voltage (J-V) characteristics under 1 sun condition of a pre-assembled DSSC is simulated in a tiberCAD based microscopic model (TCMM) along with single-diode based macroscopic model (SDMM). The calibrated model parameters are then utilized for predicting a maximum η of a DSSC belonging to an unknown electrode's thickness (L). The microscopic simulations provided a good qualitative nature of J V characteristics curves for different L and η values. A complete and best J-V curve fitting is achieved using a TCMM by incorporating an unaccounted series resistance of a FTO substrate. Particularly, model simulated J-V characteristics matches perfectly well to experimental results of a post-assembled DSSC device (η~5.46 %; L~12.0 μm) with a tolerable error (<0.1%).

Keywords: efficiency; optimization; tiberCAD; P-25; Modelling; Simulations, Dye solar cell; MATLAB; diode model; Lambert W-function

1. Introduction:

The photovoltaic solar energy is one of the most growing industries which is continuously focusing on new techniques to enhance the global efficiency of the cells and also relating the cell performance with environmental conditions [1-6]. According to literature survey mentioned in [7-9], there is a wide variety of photovoltaic cell technologies in the marketplace today, using different types of materials and can be categorized into three generations, depending on the raw material used and the level of commercial maturity. First generation photovoltaic systems use the technology of crystalline as well as multi crystalline silicon solar cells. Second generation photovoltaic systems are based on thin film amorphous silicon; cadmium telluride (CdTe); copper indium selenide (CIS) and copper, indium gallium dieseline (CIGS). Third generation photovoltaic systems include organic photovoltaic technologies that are still in progress or have not been widely marketed and new concepts in development. Dye sensitized solar cells (DSSC) are one of the suitable example of light harvesting devices falls in third generation photovoltaic technology. The first dye sensitized solar cells (DSSC) were proposed in 1991 by Michael Grätzel and Brian O'Regan. These cells belong to the group of hybrid solar cells, since they are formed by organic and inorganic materials. DSSCs have been extensively studied to minimize problems related to efficiency, cost of production and environmental issues [10-13]. The main difference of this type of cell compared to conventional solar cells is that the functional element which is responsible for the absorption of light (the dye) is separated from the transport mechanism of the charge carriers. Thus impure raw materials and simple cell processing techniques reduces the cost of the device.

Though a DSSC consists of multiple materials, yet it is a highly realized next-generation potential photovoltaic device that has been widely investigated due to its several advantageous competencies features like working even under a dim/low light and an achievable high value of η using a straightforward, cost-effective and eco-friendly manufacturing process [14]. To obtain a higher η, the key challenges are thus to enhance specific role of individual components of a DSSC viz. working electrode (WE), counter electrode (CE), an electrolyte; the bulk interfaces and various complex processes occurring in a DSSC [14-15]. Among these components, WE (charge facilitator) is the heart of a DSSC, which is a dye (photosensitizer) coated porous nanostructured thin film of TiO_2 nanoparticles or other types oxides or nano-morphologies (wire/rod/rice/tube etc.) directly or indirectly fabricated onto an optically transparent conducting oxide (FTO) substrate [16]. On light irradiation, an excited dye injects electrons into film, which diffuses or recombines until finally collected at the back of FTO substrate [17]. Since a total charge collection depends on its generation, recombination and transportation, hence a dye of suitable energy band gap with a larger optical absorbance is required. Further, losses of charge carriers needed to mimicked by optimizing kinetics role of WE, light absorptivity/energetics of dye, transportation of redox ions and charge transfer at electrode/dye/electrolyte interface [18-20].

Interestingly, rather than optimized DSSC performance (J-V characteristics and η) by unwieldy cost-time consuming repeated fabrication/assembling processes, one could predict an optimum η in advance using much faster, safer, inexpensive and reliable alternative methods like modelling and simulation techniques [21-23]. In particular, an optimum J-V characteristic and a maximum achievable η of any logical circuit based theoretical DSSC model (ideally capturing all the underlying physical processes of a real time DSSC device) could be theoretically predicted as long as necessary experimental input data of at least one pre-assembled DSSC are available for initializing the simulation process. Based on well-calibrated theoretical models, the input or output simulated results along with controlled tuneable parameters can then be used as a reference for optimizing the performance of DSSC, which help in reducing the time and the fabrication/assembling cost, as only one more post-assembling process is required to achieve an optimum DSSC device.

Here in this paper, we report the assembling and J-V characteristics of a sandwiched type DSSC assembled by a WE (L~ 3.0 μm) made from commercially available and nearly spherical shape TiO_2 nanoparticles (Degussa, P-25), an iodide /triiodide redox liquid electrolyte and photosensitizing dye N719. The measured J-V curve of assembled DSSC was generated by simulating a theoretical DSSC by TCMM-simulation (drift-diffusion of collective charge carriers) and SDMM-simulation in MATLAB (single p-n junction diode; Lambert W-function technique) [24]. The correlated and calibrated input model parameters (microscopic model: L, porosity, recombination kinetics, light absorbance of a N719 dye etc.; macroscopic model: shunt resistance ~R_S, series resistance ~R_{SH} etc.) were further utilized in controlled simulation to achieve a maximum L corresponds to an optimum η of a DSSC device. The validation of correlated simulation and experimental output parameters (V_{OC} - open-circuit voltage; J_{SC} - short-circuit photocurrent density; FF- fill factor; η; P_{MAX}- maximum power density; V_{OPT} - voltage at P_{MAX}; J_{OPT} - current density at P_{MAX}) of DSSC are discussed together with pro and cons of input parameters of theoretical models.

2. Electrode fabrication, DSSC assembling and J-V measurements

Electrode fabrication and DSSC assembling were done according to the procedure as given in reference [25]. A homogenous paste was made by mixing P-25 powder, α-terpineol and ethyl-cellulose. This paste was screen printed on commercially available F-doped SnO_2 (FTO; TEC 8) glass substrate. The TiO_2 electrode (active area ~ 1 cm^2; L~ 3.0 μm) was soaked in a 0.5 mM solution of N719 dye (acetonitrile and tert-butanol 1:1 volume ratio) for 24 hours. As received N719 dye from Solaronix has been used (no purification was done). The counter electrode was Pt-coated FTO glass substrate. Dye coated electrode were rinsed in anhydrous ethanol, dried in N_2 flow and a sandwich type DSSC has been assembled by stacking and sealing electrodes (spacer of 60 μm thickness; thermoplastic Surlyn frame) filled with a redox couple electrolyte (0.5 M 1-butyl-3-methylimidazolium iodide, 0.05 M I_2, 0.5 M 4-tert-butylpyridine (TBP) in acetonitrile). Electrical contacts were made by silver (Ag) soldering and Copper (Cu) wires. J-V characteristics of an assembled DSSC were measured under 1 sun (100 mW/cm^2, AM 1.5G) illumination with Peccell solar simulator (Model: PEL-L11). The measured output parameters (V_{OC}; J_{SC}; FF; η; P_{MAX}; V_{OPT}; J_{OPT}) of a DSSC are listed in Table-2.

3. Theoretical modelling and simulation of a DSSC structure

With the current assembling and fabrication processes of a DSSC structure, the impact of TiO_2 (L) on J-V characteristics curve is predicted and studied by a TCMM-simulation under a static1 sun light illumination. Further, it is assumed that a total charge neutrality is maintained in modelling and simulation work. The results of microscopic and macroscopic simulations are compared with the results of a real time experimental work.

One-dimensional microscopic modelling-simulation is performed in multiscale tiberCAD software in which a set of drift-diffusion equations, continuity equations, and Poisson's relation are used for facilitation of charge carriers (electrons, holes and redox ions) [26]. In this microscopic model (see Figure 1b), all injected electrons are considered from the excited state of dye only, and not from TiO_2 band gap excitation. The trapping and de-trapping of dye-injected electrons is neglected in an electrode irrespective to its L value [27]. This model consisted of two regions: 1) mesoporous electrode of TiO_2 nanoparticles surrounded by a liquid electrolyte; and 2) a liquid electrolyte in contact with a counter-electrode (covered by a thin Pt-layer) [28-30]. Optical losses caused by a liquid electrolyte are not included

and it is assumed that each absorbed photon injected one electron into conduction band of TiO_2. Moreover, it should be noted that only one dominant electron recombination loss mechanism (r_3→between TiO_2 and electrolyte; see Figure 1) is considered in the present microscopic model [31].

Macroscopic modelling-simulations are performed in MATLAB tool. A non-ideal single-diode model is used (see Figure 1c; equation 1) for keeping the simplicity and an accurate representation of simulation results (minimum error in a nonlinear J-V curve) of a DSSC structure. This model consist of: 1) a photocurrent source (J_L; depends upon light irradiance) connected in parallel with a non-ideal diode (n, ideality factor; J_0, saturated dark current density) 2) a series resistance (R_s; capturing total resistive losses within cell) and 3) a shunt resistances (R_{sh}; representing losses due to an increased conductivity at junction/edges of cell) [32]. Based on Schokley theory of a p-n junction diode, the J-V characteristics curve of such a non-ideal single-diode model [33-34] is mathematically expressed as

$$J = J_L - J_o\left[exp\left(\frac{V+JR_{sh}}{nV_T}\right) - 1\right] - \frac{V+JR_s}{R_{sh}} \quad (1)$$

where V_T is the thermal voltage. Due to implicit transcendental form of this equation 1, it is quite tedious task to extract individual diode parameters by a common least-square curve fitting method, therefore this cumbersome extraction process was made simple by changing the implicit form into an explicit form with the application of a Lambert W-function (see eqs. 2 and 3) [35].

$$J = \frac{R_{SH}(J_L+J_O)-V}{R_S+R_{SH}} - \frac{nV_T}{R_S}W(Q) \quad (2)$$

$$Q = \frac{J_O R_{Sh} R_S}{nV_T(R_S+R_{Sh})}\exp\left[\frac{R_{Sh}(R_S J_L + R_S J_O + V)}{nV_T(R_S + R_{Sh})}\right] \quad (3)$$

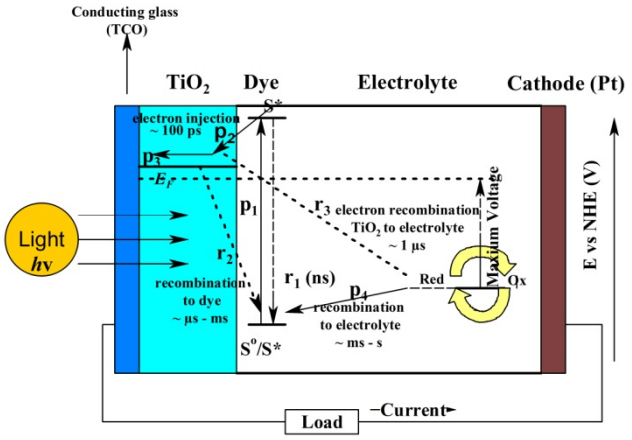

Fig.1(a) Illustration showing the working principle and the components of a DSSC structure, where dash arrows represented the various paths (time-scales) for electron loss.

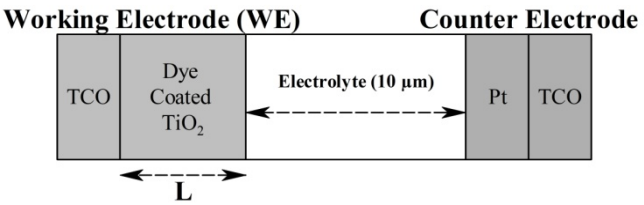

Fig.1(b) (b) 1-D microscopic DSSC model used in tiberCAD software (only significant loss mechanism r_3 of Figure 1a is used in simulation).

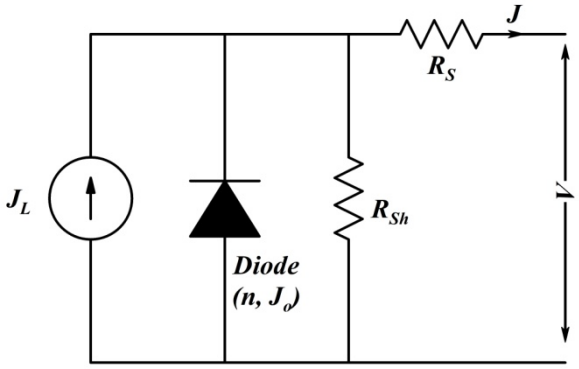

Fig.1(c) 1-D macroscopic electrical DSSC model used in MATLAB simulation.

Precautions were taken during simulations, as the accuracy of extracted input parameters (J_L, J_0, n, R_s *and* R_{sh}) depends on the choice of their initial surmise, which may tend to lead a non-convergence equation. Moreover, as the number of fitting parameters increases, the non-linear fitting method loses their ability to give the accurate results.

4. Correlations between Simulation and Experimental Results

By considering the controlled input parameters as references (see Table 1), a steady state J-V characteristics curve (see Figure 2a) was generated by simulating a 1-D microscopic DSSC device model under standard 1 sun light illumination conditions. This model consisted a WE (N719 adsorbed nanoparticles based TiO_2 electrode, active area ~ 1cm^2, L ~ 3.0 µm), a liquid redox couple electrolyte (I^-/I_3^-) and counter Pt-electrode. Along with the experimentally measured results, the simulated output DSSC parameters are listed in Table 2. A discrepancy in a FF (and η) among experimental and simulated J-V characteristics curves is clearly observed in Figure 2a, and such mismatch in FF is more pronounced in a non-linear region of J-V curves. This mismatch can be understood in terms of limitations imposed in model software, particularly neglecting the resistance contribution of a FTO substrate in a WE is one of the key limitations of TCMM (tiberCAD) simulations. Despite of an overestimation in FF, however it is clear form Table 2 that at-least V_{OC} and J_{SC} obtained through real time experiments and theoretical microscopic model-simulations matches well for a TiO_2 electrode (L ~ 3.0 µm).

Table1. Calibrated input parameters obtained by microscopic modelling–simulations of 1D DSSC model at L = 3 μm thick TiO2 electrode (see Figure 2)

SNo	Input parameters (for TCMM simulations)	Calibrated values
1	Electron relaxation rate, k_e	$0.07x10^4$ s^{-1}
2	Electron mobility, u_e	0.02 cm^2/V s
3	Iodide diff constant, D_{I^-}	8.5×10^{-6} cm^2/s
4	Triiodide diff. constant, DI_3^-	8.5×10^{-6} cm^2/s
5	Initial conc of iodide, I^-	0.45 M
6	Initial conc of triiodide, I_3^-	0.05 M
7	Recombination exponent, β	0.75
8	Cell porosity, P	0.5
9	Cell Area, A	1 cm^2

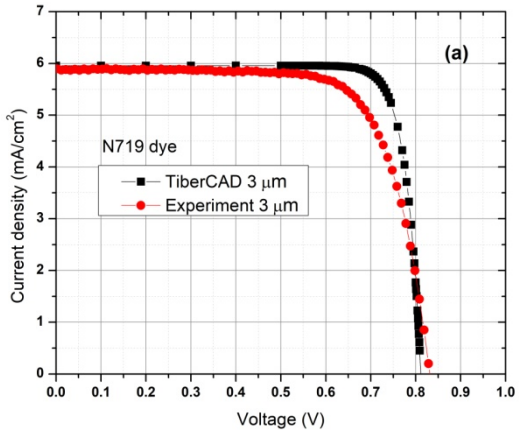

Fig.2(a)TCMM-simulation and experimental J-V characteristic curves of a DSSC at L~3.0 μm

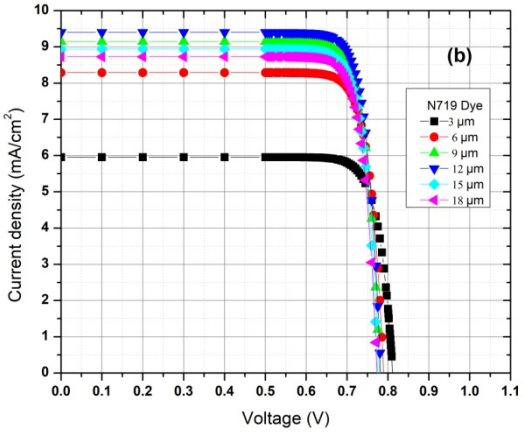

Fig. 2(b) TCMM-simulation J-V characteristic curves of a DSSC at L (3 - 18 μm).

By adapting all the calibrated input parameters of Table 1 as references, TCMM-simulation is repeated for various L (6.0 to 18.0 μm) of a WE, so that more meaningful (qualitative and quantitative) insights could be gain about the L dependency of output parameters

5. Results and Discussion

By considering results of TCCM simulation (see Figure 2b; Table 2), three more DSSC devices for different L (6.0, 9.0 and 12.0μm) of a WE are fabricated/assembled and characterized (see section 2). Experimental values together with simulated output parameters of such devices are listed in Table 2, and for quick and simple observations, their L dependency behaviors are plotted in Figures 3(a-d) and 4.

From Table 2 or Figure 3, a systematic WE (L) dependency of various DSSC output parameters (V_{OC}, J_{SC}, FF, η) is clearly noticeable i.e. an increasing J_{SC} (~5.95→9.4 $mAcm^{-2}$) with an increasing thickness (~3→12 μm) and then a decreasing J_{SC} for other higher values of thicknesses (above 12 μm). Additionally, η of a DSSC WE follows the similar tendency (see Figure 3a), while exhibiting its optimum (η ~ 6.23%) for a particular WE (L ~ 12.0 μm). Despite of having a much higher η in simulated J-V characteristics plots, above results suggested that η is indeed essentially determined by J_{SC}, and its trend is fully verified by the experimental measurements (see Figure 3; Table 2) [36]. As the light transmitted into the depth of a WE, a gradual decrease in power density of light takes place and excessive electron density becomes lower, therefore results in decrease in Voc (0.812→0.78 V) in an initial range of L, 3.0→9.0 μm [37-39]. For further increments in L (12.0 →18.0 μm), Voc shows insignificant variation [40] and settled at close to 0.78 V. Moreover, comparison of the simulated parameters with experimental measurements, the significant variation could be easily interpreted in terms of typical L dependent behaviour of J_{SC} caused by two competing simultaneous and contradictory kinetics occurring a WE i.e. generation and recombination of charge carriers in an assembled DSSC structure (See Figure 1a) [41].

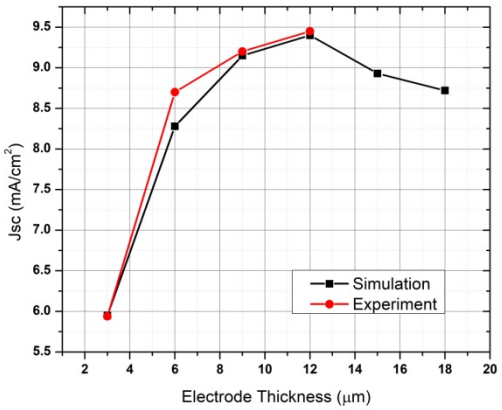

Fig. 3(a) TCMM-simulation and experimental output parameters (V_{OC}, FF, η) of a DSSC obtained under 1 sun illumination for various L of a TiO_2 electrode (area~1 cm^2).

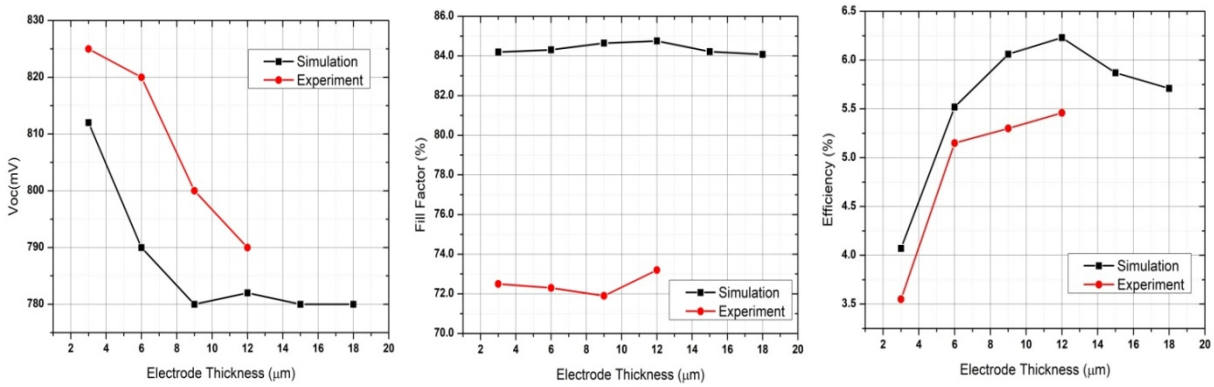

Fig. 3(b)-3(d). TCMM-simulation and experimental output parameters (V_{OC}, FF, η) of a DSSC obtained under 1 sun illumination for various L of a TiO_2 electrode (area~1 cm^2).

Table 2. Microscopic model-simulations and experimental (*) DSSC output parameters for different electrode thicknesses by taking the input reference parameters of Table 1.

Parameter	**L=3 μm**	**L=6 μm**	**L=9 μm**	**L=12 μm**	**L=15 μm**	**L=18 μm**
Jsc (mA/cm^2)	5.95/ 5.94*	8.28/8.70*	9.15/9.2*	9.4/9.45*	8.93/--	8.72/--
V_{OC} (V)	0.812/0.825*	0.79/0.82*	0.78/0.80*	0.782/0.79*	0.78/--	0.78/--
V_{OPT} (V)	0.71/0.66*	0.695/0.647*	0.685/0.63*	0.69/0.616*	0.685/--	0.68/--
J_{OPT} (mA/cm^2)	7.74/5.2*	7.943/7.97*	8.82/8.39*	9.03/8.8*	8.57/--	8.41/--
P_{MAX} (mW/cm^2)	5.495/3.432*	5.52/5.15*	6.04/5.29*	6.23/5.42*	5.87/--	5.718/--
FF (%)	84.2/72.5*	84.31/72.30*	84.65/71.9*	84.76/73.2*	84.22/--	84.08/--
η (%)	4.07/3.55*	5.52/5.15*	6.06/5.3*	6.23/5.46*	5.87/--	5.71/--

The incomplete dye covering together with a lack of light intensity deep into a thicker WE lead a gradual decrease in its J_{SC}. Besides this, a thicker WE film offers more bulk resistance at the interconnected grain boundaries of TiO_2 nanoparticles [42-43].

Based upon the above discussions i.e. a subtle balance between two opposite charge transport kinetics (see Figure 1a) and adopting the calibrated input model parameters of a reference WE (see Figure 2a; Table 1) in microscopic modelling-simulation studies, L ~12 μm (see Figure 3; Table 2 and 3; FF~84.76%; V_{OC}~ 0.782 V; J_{SC}~9.4 $mAcm^{-2}$; η~ 6.23 %; J_L~ 9.49 $mAcm^{-2}$ and R_S~29.37 $m\Omega cm^2$; see Table 2 and 3) was estimated as optimum L of a WE, as fully supported by the aligned parallel experimental measurements. Note that R_S or R_{SH} values (see Table 3) of an individual WE are estimated from a slope of J-V curve using SDMM simulations, while neglecting the contribution (resistance in R_S) of a FTO in J-V curves. Figure 3 and Table 2 clearly depict that for a particular WE (L~12 μm), the high percentage values of FF (~16%) and η (~14%) obtained in TCMM-simulations as compared to their experimental values, are consequences of assumptions made by model simulation software (tiberCAD), particularly as FTO series resistance could not be taken into simulations. Therefore, the effects of L on J-V curves are further investigated in MATLAB using SDMM-simulation with an application of a Lambert function (see Figure 1c; eqs. (1-3)). For SDMM simulations, previously as resulted TCMM-simulations and experimental J-V curves of various L are taken as inputs, and a better fitting is achieved by applying a least square fitting method within a minimum permissible error range (SSE = $8.5x10^{-7}$ to $5x10^{-6}$, R square = 0.9965 to 0.9974, RMSE = $1x10^{-4}$ to $1x10^{-3}$). The extracted macroscopic model input parameters (J_L, J_0, n, R_s and R_{sh}) for different values of L (TCMM simulated J-V characteristics; see Figure 2b) are reported and compared in Table 3. For all L of a WE, Table 3 depicts a much lower (ca. ~10^3 fold) magnitude of R_S resulted in TCMM-simulation than to its values extracted from experimental J-V curves.

Table 3. Extraction of single diode model parameters of simulated (Figure 2) and experimentally obtained J-V characteristics curves of DSSC by using SDMM-simulation performed in MATLAB. Experimentally measured value*.

L (μm)	R_s (mΩcm^2)	R_{sh} (kΩcm^2)	(n)	J_o (pA/cm^2)	J_L (mA/cm^2)
	106.6	66.95	1.389	1.024	6.087
3	11.32×10^3*	63.2*	1.432*	1.88*	5.82*
6	67.4	92.42	1.35	1.4	8.48
9	37.62	97.06	1.292	0.7	9.38
	29.37	973	1.365	2.55	9.49
12	7.07×10^3*	82.5*	1.39*	3.4*	9.44*
15	40.11	151	1.263	0.48	9.04
18	80.42	117	1.365	3.142	8.93

The drastically lowered values of R_S closely reflected a much higher FF and η for all L of a WE as reflected in all TCMM-simulations. To overcome the limitation of TCMM-simulation, the FTO resistance is considered through the combination of TCMM-simulation and SDMM-simulation, and this combined approach is referred as hybrid micro-macroscopic model simulation (HDMM-simulation).

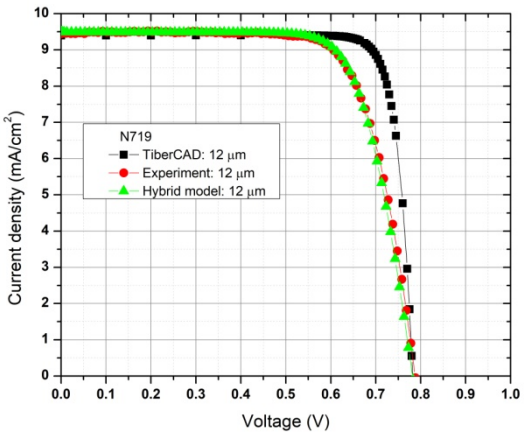

Fig.4 Experimental and TCMM-simulation J-V characteristics curves obtained under 1 sun light illumination for an optimized DSSC (L=12 μm, area~1 cm^2) along with HDMM simulation curve by considering FTO resistance (7.07x10^3 mΩcm^2).

Figure 4 shows the comparison of J-V curves among an experimental, a TCMM-simulation and a HDMM-simulation for a DSSC producing a maximum η for a particular L (ca~12μm) of a WE. It is clear that a very close fitting of

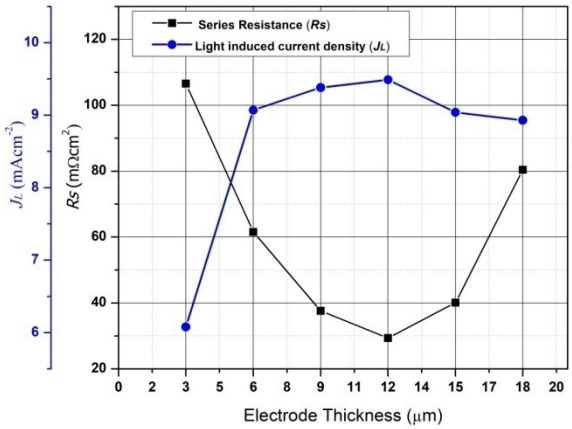

Fig 5. Thickness dependent output parameter (R_S, J_L) of a DSSC TiO_2 electrodes obtained by SDMM simulations performed in MATLAB

performance parameters of the solar cell (see Table 4) is obtained between J-V curves obtained by a real time experiment and a HDMM-simulation. Moreover, a dramatic influence a FTO resistance in R_S (unaccounted in microscopic model and a counted in macroscopic model) and curve fitting is clearly noticed**.** The last column in Table 4 shows the percentage error in HDMM-simulation with their real time measured experimental values. The maximum percentage error in η and FF is found to be ~ 0.06 % and 0.52 % respectively, between measured experimental values and HDMM simulations. Additionally, the variation of photocurrent density (J_L) with L is entirely consistent with the dependency of R_S on L value (see Figure 5). The R_S is determined to be a minimum for a particular TiO_2 electrode (L~12 μm), and this could be explained by considering the two simultaneously competing contradictory mechanisms occurring in an electrode i.e. generation and recombination of charge carriers in an assembled DSSC structure [44-45].

Increasing the thickness of WE increase the dye absorbance in the TiO_2 porous voids thus enhance the light absorbance in the photoanode and further increases the density of photo- generated carriers. Hence photo current density increases but at the same instant of time, series resistance of the electrode also tends to increase in order to affect the cell performance.

Table 4. Comparison among TCMM-simulation, Experimental and HDMM-simulation parameters for an optimized DSSC structure consisting a TiO2 electrode (thicknessL=12 μm, area ~1 cm^2).

Parameters	Microscopic simulations TCMM	Experimental results (Exp)	Hybrid Model simulations	% error Exp - TCMM	% error Exp - Hybrid model
Rs ($m\Omega cm^2$)	29	7.07×10^3	7.07×10^3	99.58	0
Jsc($m\Omega cm^2$)	9.4	9.45	9.49	0.53	0.423
V_{OC} (V)	0.782	0.79	0.783	1.012	0.886
V_{OPT} (V)	0.69	0.616	0.613	12.013	0.487
J_{OPT} (mA/cm^2)	9.03	8.8	8.92	2.613	1.363
FF (%)	84.76	73.2	73.58	15.8	0.52
η (%)	6.23	5.464	5.467	14.02	0.055

6. Conclusions

Thickness of a working electrode (WE) affected the performance of its assembled DSSC structure. TCMM-simulation depicts that as thickness increase, short-circuit photocurrent density (Jsc) firstly increases (~5.95→9.4 $mAcm^{-2}$) for electrode thickness from 3 μm to 12 μm , and achieve a maximum (9.4 $mAcm^{-2}$) at 12 μm and then decreases (9.4 $mAcm^{-2}$ -8.72 $mAcm^{-2}$) for electrode thickness from 12 μm to 18 μm. The maximum Jsc (9.4 $mAcm^{-2}$) is obtained for a 12 μm thick WE. The similar trend is observed for maximum power points and DSSC efficiency. The optimum value of value of electrode thickness is found to be consistent with the experimental results and a single diode model as well (SDMM). In general, the simulated TCMM results do not match well with the experimental observations, particularly a fill factor (error 15.8 %) and efficiency (error 14.02 %), and probably one of the possible major reasons is an unaccounted FTO resistance in simulation (tiberCAD) software. To account the FTO resistance, HDMM-simulation is carried out where the extracted value of R_S from experimental J-V curve is used along with other SDMM parameters extracted from TCMM (as input). The obtained simulated DSSC results are in close agreement with the experimental results with the tolerable permissible error for FF~0.52 % and for η~0.055 %. Henceforth, clever, feasible and well understandable modelling-simulation study just requiring initial experimental data of a preassembled DSSC device could become highly economical and beneficial to make an optimized DSSC through only and only one more additional post assembling process. It have been recently proved that the performance of the dye solar cell can be improved by developing new semiconductor absorber, counter electrodes and electro-hole transporter layers which should offer new opportunities in light harvesting areas. Photoelectrode is the critical component which determines the light harvesting capability of DSSC device. Hence by finding the high yielding routes for synthesis of various morphologies for TIO_2 nanoparticles such as nano rods and rice like structures with suitable band gap and, the efficiency

of DSSC device will be able to match with the efficiency of other type of solid state devices.

Acknowledgment

This work was supported by a SEED grant from UPES (project number UPES/RnD/122018/06).

References

[1]. Jäger-Waldau A. European photovoltaics in world wide comparison. J Non-Cryst Solids 2006;352:1922–7. doi.org/10.1016/j.jnoncrysol.2005.10.074

[2]. Parida B, Iniyan S, Goic R. A review of solar photovoltaic technologies. Renew Sustain Energy Rev 2011;15:1625–36. doi.org/10.1016/j.rser.2010.11.032

[3]. Razykov TM, Ferekides CS, Morel D, Stefanakos E, Ullal HS, Upadhyaya HM. Solar photovoltaic electricity: current status and future prospects. Sol Energy 2011;85:1580–608. doi.org/10.1016/j.solener.2010.12.002

[4]. Di Francia G. The effect of technological innovations on the cost of the photovoltaic electricity. In2015 International Conference on Renewable Energy Research and Applications (ICRERA) 2015 Nov 22 (pp. 542-546). IEEE.

[5]. Sun Y, Yan X, Yuan C, Luo H, Jiang Q. The I–V characteristics of solar cell under the marine environment: Experimental research. In2015 International Conference on Renewable Energy Research and Applications (ICRERA) 2015 Nov 22 (pp. 403-407). IEEE.

[6]. Cakmak BY. Solar energy potential of Konya and architectural design criterias for solar energy efficiency. In2015 International Conference on Renewable Energy Research and Applications (ICRERA) 2015 Nov 22 (pp. 1463-1469). IEEE.

[7]. Lacerda JS, Van Den Bergh JCJM. Diversity in solar photovoltaic energy: implications for innovation and policy. Renew Sustain Energy Rev 2016;54:331–40. doi.org/10.1016/j.rser.2015.10.032

[8]. Gangopadhyay U, Jana S, Das S. State of Art of Solar Photovoltaic Technology. In: Proceedings of International Conference on Solar Energy Photovoltaics; 2013. doi.org/10.1155/2013/764132

[9]. Busacca A, Cardona F, Caruso M, Cellura M, Cino A, Miceli R, Parisi A, Pernice R, Galluzzo FR, Viola F. Electrical characterization of low power CIGSSe photovoltaic modules. In2015 International Conference on Renewable Energy Research and Applications (ICRERA) 2015 Nov 22 (pp. 1597-1602). IEEE.

[10]. Goetzberger A, Luther J, Willeke G. Solar cells: past, present, future. Sol Energy Mater Sol Cells 2002;74:1–11 doi.org/10.1016/S0927-0248(02)00042-9

[11]. Que L., Lan Z., Wu W., Wu J., Lin J., Huang M., "High-efficiency dye-sensitized solar cells based on ultra-long single crystalline titanium dioxide nanowires". J Power Sources 2014;266:440–7. doi.org/10.1016/j.jpowsour.2014.05.022

[12]. Fitri A, Benjelloun AT, Benzakour M, Mcharfi M, Hamidi M, Bouachrine M. Theoretical design of thiazolothiazole-based organic dyes with different electron donors for dye-sensitized solar cells. Spectrochim Acta Part A: Mol Biomol Spectrosc 2014;132:232–8. doi.org/10.1016/j.saa.2014.04.164

[13]. Saha S, Das P, Chakraborty AK, Sarkar S, Debbarma R. Fabrication of DSSC with nanoporous TiO2 film and Kenaf Hibiscus dye as sensitizer. International Journal of Renewable Energy Research (IJRER). 2016 Jun 18;6(2):620-7.

[14]. Kay A, Grätzel M. Low cost photovoltaic modules based on dye sensitized nanocrystalline titanium dioxide and carbon powder. Solar Energy Materials and Solar Cells. 1996 Oct 30;44(1):99-117. doi.org/10.1016/0927-0248(96)00063-3

[15]. Smestad G, Bignozzi C, Argazzi R. Testing of dye sensitized TiO_2 solar cells I: Experimental photocurrent output and conversion efficiencies. Solar energy materials and solar cells. 1994 Mar 1;32(3):259-72. doi.org/10.1016/0927-0248(94)90263-1

[16]. Chou CS, Hsiung CM, Wang CP, Yang RY, Guo MG. Preparation of a counter electrode with P-type NiO and its applications in dye-sensitized solar cell. International Journal of Photoenergy. 2010;2010. dx.doi.org/10.1155/2010/902385

[17]. Gong J, Sumathy K, Zhou Z, Qiao Q. Modeling of interfacial and bulk charge transfer in dye-sensitized solar cells. Cogent Engineering. 2017 Jan 1;4(1):1287231. dx.doi.org/10.1080/23311916.2017.1287231

[18]. Thavasi VR, Renugopalakrishnan V, Jose R, Ramakrishna S. Controlled electron injection and transport at materials interfaces in dye sensitized solar cells. Materials Science and Engineering: R: Reports. 2009 Jan 29;63(3):81-99. doi.org/10.1016/j.mser.2008.09.001

[19]. Grätzel M. Conversion of sunlight to electric power by nanocrystalline dye-sensitized solar cells. Journal of Photochemistry and Photobiology A: Chemistry. 2004 Jun 1;164(1-3):3-14. doi.org/10.1016/j.jphotochem.2004.02.023

[20]. Tripathi B, Yadav P, Kumar M. Charge transfer and recombination kinetics in dye-sensitized solar cell using static and dynamic electrical characterization techniques. Solar Energy. 2014 Oct 1;108:107-16. doi.org/10.1016/j.solener.2014.06.037

[21]. Onodera M, Ogiya K, Suzuki A, Tsuboi H, Hatakeyama N, Endou A, Takaba H, Kubo M, Miyamoto A. Modeling of dye-sensitized solar cells based on TiO2 electrode structure model. Japanese Journal of Applied Physics. 2010 Apr 20;49(4S):04DP10. dx.doi.org/10.1143/JJAP.49.04DP10TI

[22]. Ni M, Leung MK, Leung DY. Theoretical modelling of the electrode thickness effect on maximum power point of dye-sensitized solar cell. The Canadian Journal of Chemical Engineering. 2008 Feb;86(1):35-42. doi.org/10.1002/cjce.20015

[23]. Supriyanto E, Kartikasari HA, Alviati N, Wiranto G. Simulation of Dye-Sensitized Solar Cells (DSSC) Performance for Various Local Natural Dye Photosensitizers. InIOP Conference Series: Materials Science and Engineering 2019 Apr (Vol. 515, No. 1, p. 012048). IOP Publishing. doi:10.1088/1757-899X/515/1/012048

[24]. Jain A, Kapoor A. Exact analytical solutions of the parameters of real solar cells using Lambert W-function. Solar Energy Materials and Solar Cells. 2004 Feb 6;81(2):269-77. doi.org/10.1016/j.solmat.2003.11.018

[25]. Parmar KP, Ramasamy E, Lee J, Lee JS. Rapid (~ 10 min) synthesis of single-crystalline, nanorice TiO_2 mesoparticles with a high photovoltaic efficiency of above 8%. Chemical Communications. 2011;47(30):8572-4. Doi.org/10.1039/C1CC12150B

[26]. Gagliardi, A., Auf der Maur, M., Pecchia, A., & Di Carlo, A. (2009). Dye Solar Cell Simulations Using Finite Element Method. 2009. 13th International Workshop on Computational Electronics. DOI:10.1109/iwce.2009.5091107

[27]. Rudra S, Sarker S, Kim DM. Review on simulation of current–voltage characteristics of dye-sensitized solar cells. Journal of Industrial and Engineering Chemistry. 2019 Aug 20. doi.org/10.1016/j.jiec.2019.08.030

[28]. Penny M, Farrell T, Please C. A mathematical model for interfacial charge transfer at the semiconductor–dye–electrolyte interface of a dye-sensitised solar cell. Solar Energy Materials and Solar Cells. 2008 Jan 1;92(1):11-23. doi.org/10.1016/j.solmat.2007.07.013

[29]. Thomas S, Deepak TG, Anjusree GS, Arun TA, Nair SV, Nair AS. A review on counter electrode materials in dye-sensitized solar cells. Journal of

Materials Chemistry A. 2014;2(13):4474-90. DOI: 10.1039/c3ta13374e

[30].Grätzel M. Dye-sensitized solar cells. Journal of photochemistry and photobiology C: Photochemistry Reviews. 2003 Oct 31;4(2):145-53. doi.org/10.1016/S1389-5567(03)00026-1

[31]. Oda T, Tanaka S, Hayase S. Differences in characteristics of dye-sensitized solar cells containing acetonitrile and ionic liquid-based electrolytes studied using a novel model. Solar energy materials and solar cells. 2006 Oct 16;90(16):2696-709. doi.org/10.1016/j.solmat.2005.11.013

[32]. Ferber J, Stangl R, Luther J. An electrical model of the dye-sensitized solar cell. Solar Energy Materials and Solar Cells. 1998 May 12;53(1-2):29-54. doi.org/10.1016/S0927-0248(98)00005-1

[33]. Diantoro M, Suprayogi T, Hidayat A, Taufiq A, Fuad A, Suryana R. Shockley's Equation Fit Analyses for Solar Cell Parameters from IV Curves. International Journal of Photoenergy. 2018;2018. *2018*.doi.org/10.1155/2018/9214820

[34] Ahmed MT, Gonçalves T, Tlemcani M. Single diode model parameters analysis of photovoltaic cell. In2016 International Conference on Renewable Energy Research and Applications (ICRERA) 2016 Nov 20 (pp. 396-400). IEEE.

[35]. Ghani F, Duke M. Numerical determination of parasitic resistances of a solar cell using the Lambert W-function. Solar Energy. 2011 Sep 1;85(9):2386-94. doi.org/10.1016/j.solener.2011.07.001

[36]. Tsai JK, Hsu WD, Wu TC, Meen TH, Chong WJ. Effect of compressed TiO_2 nanoparticle thin film thickness on the performance of dye-sensitized solar cells. Nanoscale research letters. 2013 Dec;8(1):459. doi.org/10.1186/1556-276X-8-459

[37]. Kao MC, Chen HZ, Young SL, Kung CY, Lin CC. The effects of the thickness of TiO2 films on the performance of dye-sensitized solar cells. Thin Solid Films. 2009 Jul 1;517(17):5096-9. doi.org/10.1016/j.tsf.2009.03.102

[38]. Balraju P, Suresh P, Kumar M, Roy MS, Sharma GD. Effect of counter electrode, thickness and sintering temperature of TiO_2 electrode and TBP addition in electrolyte on photovoltaic performance of dye sensitized solar cell using pyronine G (PYR) dye. Journal of Photochemistry and photobiology A: Chemistry. 2009 Jul 5;206(1):53-63. doi.org/10.1016/j.jphotochem.2009.05.014

[39]. Miyasaka T, Kijitori Y, Murakami TN, Kimura M, Uegusa S. Efficient nonsintering type dye-sensitized photocells based on electrophoretically deposited TiO_2 layers. Chemistry Letters. 2002 Dec 5;31(12):1250-1. doi.org/10.1246/cl.2002.1250

[40]. Gómez R, Salvador P. Photovoltage dependence on film thickness and type of illumination in nanoporous thin film electrodes according to a simple diffusion model. Solar Energy Materials and Solar Cells. 2005 Sep 15;88(4):377-88. doi.org/10.1016/j.solmat.2004.11.008

[41]. Zhao W, Bala H, Chen J, Zhao Y, Sun G, Cao J, Zhang Z. Thickness-dependent electron transport performance of mesoporous TiO2 thin film for dye-sensitized solar cells. Electrochimica Acta. 2013 Dec 30;114:318-24. doi.org/10.1016/j.electacta.2013.09.165

[42]. Park KH, Kim TY, Kim JH, Kim HJ, Hong CK, Lee JW. Adsorption and electrochemical properties of photoelectrodes depending on TiO_2 film thickness for dye-sensitized solar cells. Journal of Electroanalytical Chemistry. 2013 Nov 1;708:39-45. doi.org/10.1016/j.jelechem.2013.09.014

[43]. Docampo P, Guldin S, Steiner U, Snaith HJ. Charge transport limitations in self-assembled TiO_2 photoanodes for dye-sensitized solar cells. The journal of physical chemistry letters. 2013 Feb 12;4(5):698-703. doi.org/10.1021/jz400084n

[44]. Oktiawati UY, Mohamed NM, Burhanudin ZA. Simulation on the performance of dye solar cell incorporated with TiO_2 passivation layer. International Journal of Photoenergy. 2016;2016. dx.doi.org/10.1155/2016/8507625

[45]. Kumari JM, Sanjeevadharshini N, Dissanayake MA, Senadeera GK, Thotawatthage CA. The effect of TiO_2 photo anode film thickness on photovoltaic properties of dye-sensitized solar cells. Ceylon Journal of Science. 2016 Jun 22;45(1).dx.doi.org/10.4038/cjs.v45i1